Agriculture, Ecosystems and Environment 294 (2020) 106883

Contents lists available at ScienceDirect

Agriculture, Ecosystems and Environment

journal homepage: www.elsevier.com/locate/agee

Agriculture driven nitrogen wet deposition in a karst catchment in southwest China

Jie Zeng[a], Fu-Jun Yue[b,c,d,*], Si-Liang Li[b,e,f], Zhong-Jun Wang[c,f], Cai-Qing Qin[b], Qi-Xin Wu[g], Sheng Xu[b]

[a] Institute of Earth Sciences, China University of Geosciences (Beijing), Beijing 100083, China
[b] Institute of Surface-Earth System Science, Tianjin University, Tianjin 300072, China
[c] State Key Laboratory of Environmental Geochemistry, Institute of Geochemistry, Chinese Academy of Sciences, Guiyang 550081, China
[d] School of Geographical and Earth Sciences, University of Glasgow, Glasgow G12 8QQ, United Kingdom
[e] Tianjin Key Laboratory of Earth Critical Zone Science and Sustainable Development in Bohai Rim, Tianjin University, Tianjin 300072, China
[f] Puding Karst Ecosystem Research Station, Institute of Geochemistry, Chinese Academy of Sciences, Anshun 562100, China
[g] Key Laboratory of Karst Environment and Geohazard, Ministry of Land and Resources, Guizhou University, Guiyang 550025, China

ARTICLE INFO

Keywords:
Nitrogen flux
Nitrate isotopes
Rainwater
Carbonate rock area
Agriculture-related microbial nitrogen cycle

ABSTRACT

Nitrogen (N) deposition plays a key role in ecosystem function as one of the major N sources for natural vegetation, particularly in karst agricultural areas with thin soil cover, which drive the karst N fate via rainwater. To understand the seasonal and spatial variation in nitrogen deposition and to identify the major sources of nitrate in wet deposition in a karst agricultural area (Houzhai Catchment) in southwestern China, two sites with different land use were selected to assess wet and dry deposition for one year. Houzhai village (HZV) is an area highly influenced by agriculture, whereas Muzhu reservoir (MZR) is a more pristine environment with less anthropogenic influence. Nitrogenous species and dual nitrate isotopes were analyzed. The results showed that agriculture-derived NH_4^+ was the major contributor of annual total wet N deposition (> 55 %). The contribution of NH_4^+ to wet N deposition was 1.63 times higher than that of NO_3^- and dissolved organic nitrogen (DON). The annual nitrogen deposition in this study was approximately twice as much as the average wet N deposition over China, while lower dry N deposition relative to other Chinese monitoring sites was observed. The $\delta^{15}N\text{-}NO_3^-$ showed a seasonal trend of negative summer values and positive winter values, which were primarily controlled by the variations in NO_x emission sources. Seasonal variation in $\delta^{18}O\text{-}NO_3^-$ was mainly controlled by NO_x oxidation pathways and showed a similar trend to $\delta^{15}N\text{-}NO_3^-$. The contributions from four endmembers (coal combustion, vehicle exhaust, biomass burning, and soil emission) were calculated using a stable isotope mixing model. Contributions show a clear seasonal variation (except vehicle exhaust), with the four sources accounting for 20.0 %, 25.6 %, 22.9 % and 31.5 % respectively (annual mean probability estimate, AMPE) at HZV, and 19.0 %, 27.8 %, 23.2 % and 30.0 % (AMPE) at MZR. Isotopic evidence determined agricultural soil emission is a major contributor to rainwater during the summer growing season, which can significantly impact the agricultural ecosystems.

1. Introduction

In recent decades, nitrogen (N) in the environment has dramatically increased as a result of the intensive use of fossil fuels and application of fertilizers, which has significantly impacted on the global N cycle (Galloway et al., 2008; Wei et al., 2019a), for example by increasing the flux of NO_x ($NO + NO_2$) and NH_3 into the atmosphere. Generally, agricultural processes, including fertilization and straw burning, contribute large amount of gaseous nitrogen-containing compounds to the atmosphere (Wang et al., 2020; Zeng et al., 2019), e.g., NH_3 volatilization from soil after fertilization and NO_x emission from soil-microbial nitrification/denitrification. The high concentration of NO_x and NH_3 in the atmosphere which subsequently become dissolved in rainfall as compounds including nitrate (NO_3^-), ammonium (NH_4^+) and dissolved organic N (DON)) directly result in high levels of atmospheric N deposition (Kendall et al., 2007). Excess N deposition has attracted great societal concern about negative impacts on ecosystem health and services (Bobbink et al., 2010; Gao et al., 2019; Liu et al., 2017a). This

* Corresponding author at: Institute of Surface-Earth System Science, Tianjin University, Tianjin 300072, China.
E-mail addresses: fujun_yue@tju.edu.cn, junyuefu@163.com (F.-J. Yue).

https://doi.org/10.1016/j.agee.2020.106883
Received 8 May 2019; Received in revised form 19 February 2020; Accepted 21 February 2020
Available online 25 February 2020

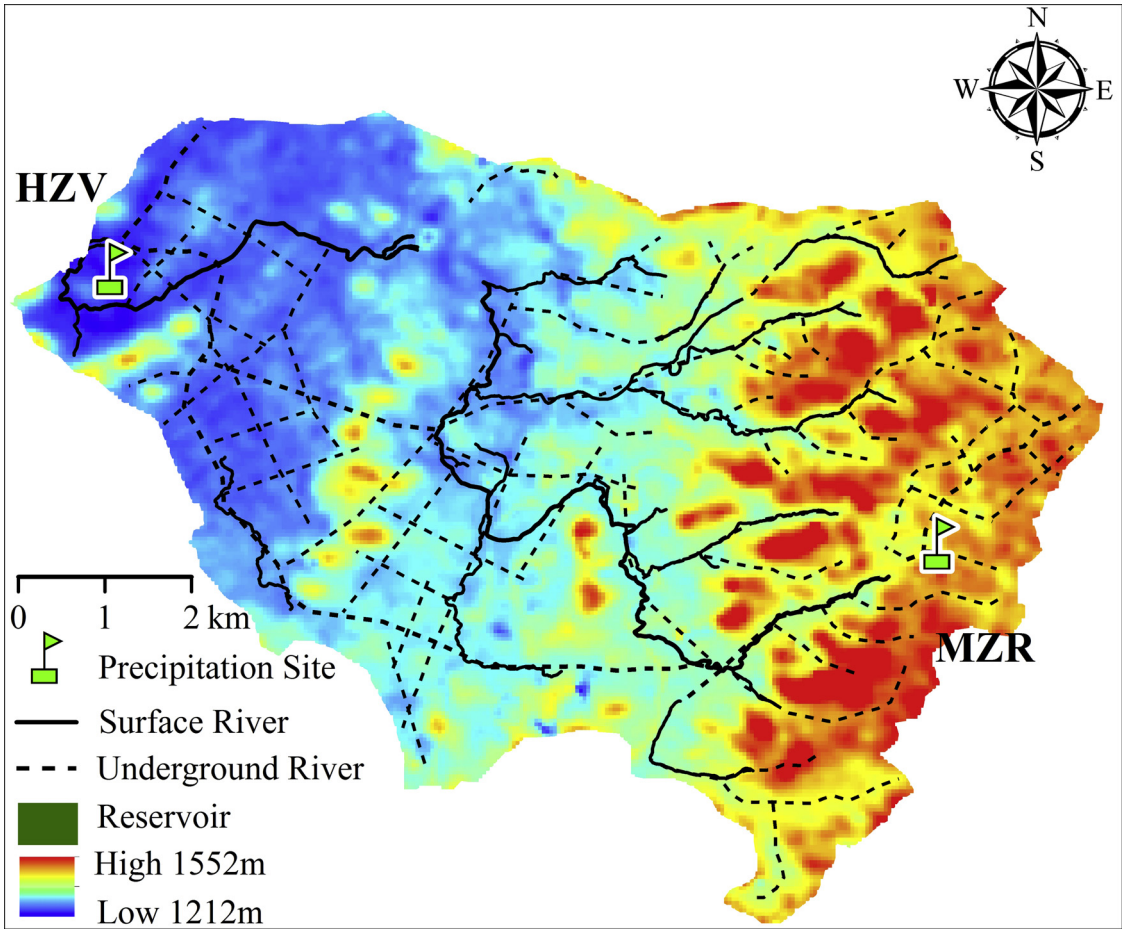

Fig. 1. Sampling sites in Houzhai Catchment. Map modified from Zhang et al. (2017).

phenomenon is particularly prominent in countries undergoing rapid agricultural development, like China (Liu et al., 2013; Yu et al., 2019; Zhang et al., 2008). As N is an essential biological element in most ecosystems, excessive N deposition is considered to be a crucial environmental factor disturbing the structure and function of surface-earth ecosystems, particularly in vulnerable environments, such as karst agricultural regions (Erisman et al., 2007; Liu et al., 2017b; Zeng et al., 2019).

In karst areas of southwestern (SW) China, the typical geomorphology is carbonate cone-cockpit terrain with thin discontinuous soil cover. The climate is subtropical monsoonal with the majority of rainfall occurring during the wet season, which results in low nutrient levels in the epikarst system. Thus, nitrogen deposition in this area is important to the development of the ecosystem and rock weathering due to the low pH of the rainfall. The N level of karst aquatic ecosystems is therefore sensitive to N deposition originating from agricultural production (e.g. fertilization and straw burning) (Yue et al., 2015). Recent studies have found that rainfall drives N transport in agricultural karst aquifer systems (Wang et al., 2020; Yue et al., 2019). Thus, rainfall can be considered as one of driving factors for karst N fate as it is an important nitrogen source for the surface ecosystem (Gao et al., 2019; Wang et al., 2020). Additionally, high rates of short-term N deposition may accelerate plant growth and affect the stability of the agroecosystem (Bobbink et al., 2010; Lee et al., 2012). Therefore, the evaluation of N deposition rates and N source identification is critical to understanding the N cycle in karst areas.

Generally, NO_3^- and NH_4^+ from atmospheric deposition originate from gas-phase inorganic N (NO_x and NH_3), which can have many origins (e.g. NO_x and NH_3 from coal combustion, vehicle exhaust and biomass burning, NH_3 from animal waste and fertilizer volatilization, and NO_x from soil emissions) (Chang et al., 2018; Felix et al., 2013, 2012; Li and Wang, 2008; Walters et al., 2015a). Additionally, a series of studies have suggested that DON in atmospheric deposition can also be derived from natural sources (e.g., sea spray droplets and plant pollen) as well as anthropogenic sources (primary emissions from biomass burning and fertilizers, and secondary production from gas phase reactions of inorganic N and non-nitrogenous organic matter, e.g. NO_x and VOCs) (Jang and Kamens, 2001; Lee et al., 2012; Liu et al., 2017b). However, there are many uncertainties in quantifying the sources of nitrogen, and its behavior in atmospheric deposition via the traditional analysis method of nitrogen concentration.

Stable nitrogen isotopic analysis provides an effective tool for the study of the atmospheric nitrogen cycle (Kendall et al., 2007; Kawashima and Kurahashi, 2011). Stable isotope studies have clearly suggested that a major control on ammonium in agricultural areas is volatilization of fertilizers (Xiao et al., 2012; Xie et al., 2008). However, confidently identifying nitrate sources can be difficult due to the range of sources and complexity of photochemical processes occurring during formation. For example, previous studies have used dual isotopes of nitrate (expressed as $\delta^{15}N$ and $\delta^{18}O$ values) to investigate atmospheric nitrogen deposition and its sources (Li et al., 2020; Liu et al., 2017b; Nelson et al., 2018), and found that nitrate isotopic composition in rainwater can be affected by the transformation of gas-phase nitrogen oxides (NO_x, the precursor of nitrate in rainwater) and variations in NO_x sources (Felix et al., 2012; Fibiger and Hastings, 2016; Walters et al., 2015a).

Dual nitrate isotopes have been successfully applied to understand atmospheric nitrogen transfer, spatial-temporal variations, and source apportionment in urban areas or developed regions (Elliott, et al., 2019; Li et al., 2020; Liu et al., 2017b) and agricultural areas (Hall et al.,

2016; Jin et al., 2019; Lee et al., 2012). However, there are few studies comparing N deposition mechanisms and sources between rural and urban areas. In order to know the N deposition level and understand the fate of N deposition in a karst agriculture area, the concentrations of N species and dual nitrate isotopes were analyzed in rainwater samples, which were collected at two sites with different land uses in a karst agricultural catchment in SW China. The main objective of present study is to identify the nitrogen wet deposition process and its controlling factors and sources. Moreover, the quantitative assessment of rainwater nitrate sources will make a complete estimation of atmospheric nitrate sources from the perspective of anthropogenic and activities natural process in frequent-rainy karst area with extensive agricultural production. This study will powerful support policy makers N management strategies to mitigate nitrogen contamination in SW China, Particularly the agricultural N management.

2. Materials and methods

2.1. Site description

Based on landscape and land use, two sites located in Houzhai Catchment (HZ) were chosen to collect samples for dry and wet deposition measurements (Fig. 1). One site representing lesser anthropogenic influence is located at Muzhu Reservoir in the mountainous area located in the headwaters of HZ catchment, with land-use comprising shrub, forest and little agricultural (paddy) land (MZR, 105°46′47″E, 26°14′04″N, 1330 m asl.). The second site at Houzhai village represents greater anthropogenic influence and is located in the flat plains of the lower reaches of the HZ catchment within a mixed area of buildings and agricultural land (dry land and paddy fields) (HZV, 105°41′15″E, 26°16′09″N, 1220 m asl.). The HZ catchment has an area of 73.4 km^2 and is in the center of the karst region in Guizhou Province, SW China. The catchment has been intensively studied since 1978 as an area representative of cone and cockpit karst geomorphology (Zhang et al., 2017; Qin et al., 2019). Elevation decreases from southeast to northwest, ranging from 1212 to 1552 m.

This catchment is a characterized by a subtropical, monsoonal climate, with an average annual temperature of 20.1℃. Annual precipitation ranges from 1200 to 1400 mm, with the majority of annual rainfall (~80 %) occurring during the wet season (May to October). The climate in the study catchment can be divided into spring (March to May), summer (June to August), autumn (September to November), and winter (December to February of the following year). The lithology is composed of Permian and Triassic limestone and dolomite (Chen et al., 2008; Zhang et al., 2017); they develop into limestone soil (Rendzina) according to FAO soil taxonomy classifications (IUSS Working Group WRB, 2015), which correspond to Mollic Inceptisols (Liu et al., 2020).

Land cover/use includes natural vegetation (forest, shrub & grass), aquatic areas (rivers & reservoirs), developed areas (road & built-up areas), farmland (dry land & paddy fields) and bare rock (Liu et al., 2016; Yue et al., 2019). The farmland (dry land & paddy field) is mostly distributed in the middle and lower reaches and covers approximately 41 % of the area, and approximately two thirds of the agricultural land is covered by rice paddies in the wet season (Oliver et al., 2020; Yue et al., 2019). Other crops grown in the catchment are corn and various vegetables. Canola and selected vegetables are the main crops in the dry season. In the study catchment, various fertilizers including synthetic fertilizers, urea, di-ammonium phosphate and animal waste are applied for crop growth (Liu et al., 2020). Animal waste (e.g. pig and cattle manure) is seasonally used as a fertilizer at the beginning of major crop tillage periods (Yue et al., 2019), such as for rice (summer crop, May) and rape (winter crop, November), while the other fertilizers are typically further applied during April ~ July. Overall, the generally percentage of fertilizer use of urea, di-ammonium phosphate and animal waste are approximately 40–60 %, 20–30 %, and 20–30 %, respectively.

2.2. Sample collection

Precipitation samples were collected from June 2016 to May 2017. Rainwater samples were collected using a 65 cm diameter polyethylene sampler placed approximately 100 cm above the ground. A polyethylene cap was used to avoid particle fallout in the absence of rain for wet deposition. Wet deposition samples were collected daily, while dry deposition samples were collected monthly using the same size polyethylene sampler at the beginning of each month. When it began to rain, the cap was removed as quickly as possible from the wet deposition sampler and closed for the dry deposition sampler. A total of 86 and 90 wet deposition samples were collected at HZV and MZR, respectively, and 12 dry deposition samples were collected at each site.

2.3. Analysis and calculation

Electrical conductivity and pH were measured immediately with a portable multiple parameter meter (WTW, Multi Line 3320). The precipitation samples were then filtered through 0.45 μm acetate membrane filters, and the filtrate was stored directly in a pre-cleaned polyethylene bottle for measurement of nitrogen concentration and dual isotopes of nitrate. All the wet deposition samples were kept refrigerated at 4℃ until analysis. The NH_4^+–N, NO_3^-–N + NO_2^-–N and dissolved total nitrogen (DTN) concentration ([N]) in rainwater samples were analyzed by using a continuous-flow analyzer (Skalar, SAN^{+} $^{+}$). The contribution from [NO_2^-–N] to [NO_3^-–N + NO_2^-–N] is less than 1%, which indicated that NO_2^-–N contribution is insignificant and will not be discussed. Dissolved organic nitrogen (DON) was calculated by subtracting [NH_4^+–N] and [NO_3^-–N + NO_2^-–N] from DTN. The volume-weighted mean (VWM) N concentrations of NH_4^+–N, NO_3^-–N, DON and DTN were calculated by dividing the sum of products of N concentration and precipitation amount with the sum of precipitation amount recorded for the events, and the N wet deposition rate (kg ha^{-1} yr^{-1}) was calculated with the VWM concentration and precipitation amount. The N dry deposition rate was calculated by nitrogen content (expressed as %) of dry deposition samples measured using an elemental analyzer (Perkin Elmer, PE-2400) and the sampler area. The denitrifier method was used to measure nitrate isotopes of the samples (Mcilvin and Casciotti, 2011) based on its nitrate concentrations, and the monthly δ^{15}N-NO_3- and δ^{18}O-NO_3- values were the mean value of each month. In brief, the denitrifier (*Pseudomonas chlororaphis* subsp. aureofaciens ATCC 13985, which lacks an N_2O-reductase enzyme, was used to convert NO_3^- into N_2O. N_2O was then purified by using on-line pre-concentration ability of trace gases, and the δ^{15}N and δ^{18}O analysis of the N_2O was performed simultaneously using an isotope ratio mass spectrometer (IsoPrime, GV, UK). The isotope ratios of N_2O are expressed in delta (δ) notation, i.e., δ (‰) = [$R_{sample}/R_{standard}$ – 1] × 1000, where R_{sample} is $^{15}N/^{14}N$ or $^{18}O/^{16}O$ of sample, $R_{standard}$ is the ^{15}N ratios in atmospheric N_2 or ^{18}O ratios in Vienna Standard Mean Ocean Water. In order to ensure the reliability of isotope analysis, the international reference materials (USGS-32, USGS-34, USGS-35 and IAEA-N3) with same treatment as samples were used for calibration of $\delta^{15}N_{nitrate}$ and $\delta^{18}O_{nitrate}$ after blank correction (Mcilvin and Casciotti, 2011). In general, analytical precision of δ^{15}N and δ^{18}O for nitrate were better than ± 0.3‰ and ± 0.5‰, respectively. Then a Bayesian isotope mixing model (SIAR; details in Supplementary Information (SI)) was used to quantify the dominant N sources for wet deposition of NO_3^- (Jin et al., 2018; Moore and Semmens, 2008; Parnell et al., 2010). SIAR model was performed with the residual error and process error term as well as uninformative priors. Residual error explains the unknown sources of variability in the mixture progress (Stock and Semmens, 2016). The model result provides the posterior probability distribution of the proportional contribution of the different sources and reports overview statistics including median, mean, standard deviation, and

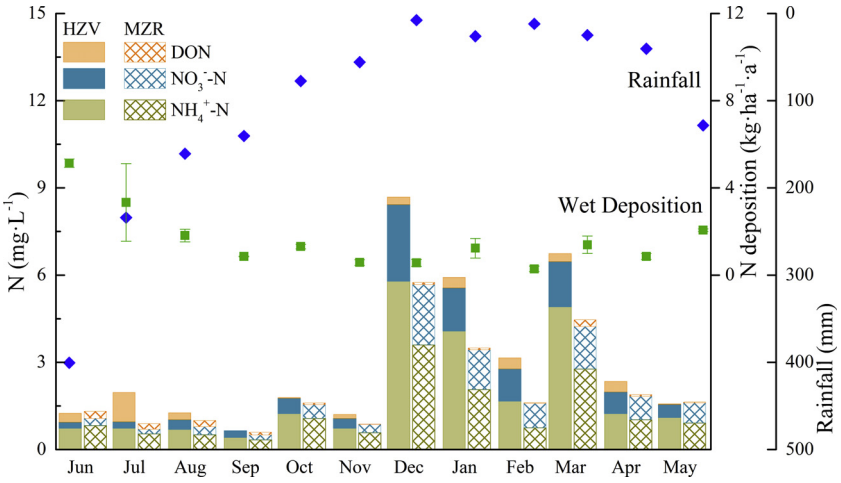

Fig. 2. The concentration of nitrogenous species, nitrogen wet deposition and rainfall in Houzhai Catchment, southwestern China.

credible interval (Li et al., 2020).

3. Results

3.1. The concentration of nitrogenous species at two karstic sites

The total annual rainfall during the study period was 1308.5 mm. The annual VWM concentrations of NH_4^+–N, NO_3^-–N, DON and DTN were 0.9, 0.3, 0.3, and 1.5 mg L^{-1} in HZV and 0.7, 0.3, 0.2 and 1.2 mg L^{-1} in MZR, respectively (Fig. 2, Tables S1 and S2). The trends in monthly N concentration are different between the two sites, but the highest NH_4^+–N and NO_3^-–N concentration were all observed in December when the highest DTN concentrations were observed (Fig. 2). The monthly contribution from NH_4^+–N to wet N deposition ranged from 37.8 to 72.9 % at HZV and from 47.0 to 66.9 % at MZR (Fig. 2). The monthly contribution of NO_3^-–N ranged between 10.6 and 35.0 % at HZV and from 18.4 to 53.0% at MZR, with the highest values in February and relatively lower values in June and July. The contribution of DON was less than 20 %, except in July at HZV (Fig. 2).

On the basis of monthly precipitation and VWM concentration of DTN, the annual wet N deposition rates between 2016 and 2017 were 21.8 and 17.1 kg ha^{-1} yr^{-1} in HZV and MZR (Tables S1 and S2), respectively. Including the contribution of dry deposition, the total nitrogen deposition is 25.2 at HZV and 18.3 kg ha^{-1} yr^{-1} at MZR, with an average of 21.8 kg ha^{-1} yr^{-1}. The highest monthly wet N deposition was observed in June at both sites (5.0 kg ha^{-1} yr^{-1} at HZV and 5.3 kg ha^{-1} yr^{-1} at MZR) owing to the high intensity rainfall during this month, which contributed 22.9 and 31.0 % to the annual wet N deposition, respectively.

The average molar ratios of NH_4^+/NO_3^- are 2.7 at HZV and 2.2 at MZR (Tables S1 and S2). The lowest and highest NH_4^+/NO_3^- ratios were observed at HZV in February (1.5) and June (3.7), respectively. The NH_4^+/NO_3^- ratios at MZR showed seasonal variation with low values in the dry season (0.9–1.9, December to May of the following year) and high values in the wet season, particularly in June (3.3).

3.2. The isotopic values of nitrate

At HZV the monthly $\delta^{15}N\text{-}NO_3^-$ values range from −9.0 ‰ (July) to +2.4 ‰ (February) with mean a value of −2.8 ‰, which is slighter narrower than at MZR where values range from −9.1 ‰ (July) to +2.5 ‰ (February), with a mean value of −2.7 ‰ (Tables S1 and S2). The monthly mean $\delta^{18}O\text{-}NO_3^-$ values of rainwater at HZV ranged from +54.2‰ (July) to +75.8 ‰ (February) and from +54.5‰ (July) to +75.3 ‰ (February) at MZR, (Tables S1 and S2).

4. Discussion

4.1. Concentrations of N in rainwater and N deposition rate

The annual inorganic N concentrations observed in our study were much higher than those for forested areas in South China (0.02–0.05 mg L^{-1} for NH_4^+–N and 0.02–0.08 mg L^{-1} for NO_3^-–N) (Chen and Mulder, 2007) and karst virgin forest in SW China (0.4 mg L^{-1} for NH_4^+–N and 0.04 mg L^{-1} for NO_3^-–N) (Zeng et al., 2020). Additionally, our values are higher than previously reported values (0.5 mg L^{-1} for NH_4^+–N and 0.2 mg L^{-1} for NO_3^-–N) for Puding county (Lü et al., 2017; Wu et al., 2012), which is close to the studied area. This could be attributed mainly to the fact that the sampling frequency in the current study is much higher than that of previous studies, and all the rainfall events were sampled as frequently as possible, particularly small rainfall events with relatively high N concentration. The location of sample sites in an agricultural area may be another contributing factor. Higher monthly NH_4^+–N and NO_3^-–N concentrations were observed at HZV compared with the values at MZR (Fig. 2, Tables S1 and S2), which suggests that there is higher loading of nitrogenous species at HZV, derived from agricultural activities and relatively denser residents.

The concentrations of NH_4^+–N and NO_3^-–N during winter and spring were higher than those in summer and autumn, due to the lower precipitation and rainfall frequency. In the late autumn and winter, more gaseous nitrogen compounds (NO_x and NH_3) will be accumulated in the atmosphere with increased heating of dwellings (coal combustion) in these seasons, which will subsequently result in higher levels of NO_3^- and NH_3 or NH_4^+ in particulates (Yeon et al., 2015). Although the low rainfall intensity/frequency in winter cannot wash out nitrogen completely from particulate matter (Wei et al., 2019b), it can capture a proportion, which would result in high concentrations of nitrogenous species (NH_4^+–N and NO_3^-–N) in wet deposition (Elliott et al., 2015). It is also evident that the secondary annual peak of NH_4^+–N and NO_3^-–N concentration occurs in March, which is indicative of more atmospheric NH_3 and NO_x being deposited by rain droplets, as there was double the rainfall in March compared with February. The variation in DON concentration didn't show seasonal variation, suggesting that it is affected by more factors (Fig. 2), such as the organic nitrates derived from gas phase reactions and N existing in reduced states including urea, amino acids, and amines from biomass combustion and agricultural production (Lee et al., 2012).

The annual wet N deposition calculated from this study is 1.63 times higher than the average annual wet N deposition over China (13.7 kg ha^{-1} yr^{-1}) (Zhu et al., 2015), but similar to the values obtained for another subtropical Chinese catchment with cultivated land covering

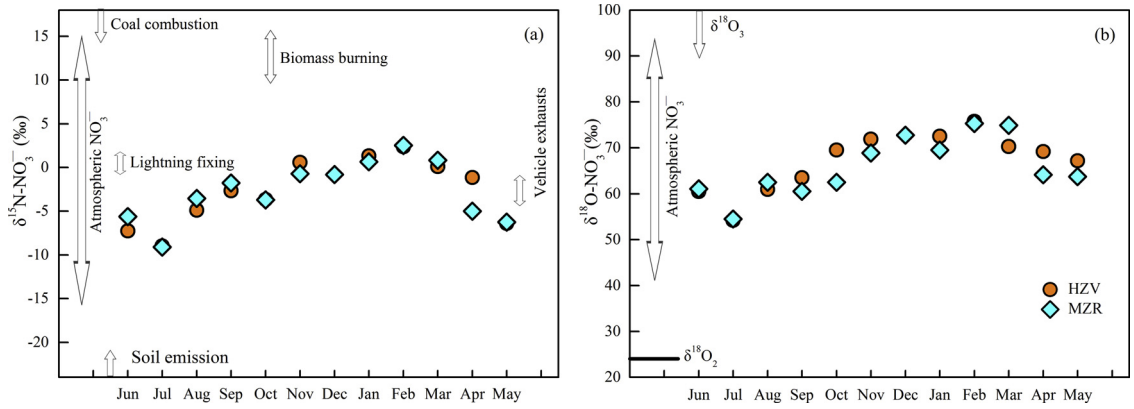

Fig. 3. (**a**) Seasonal variation of monthly δ^{15}N-NO_3^- values, and (**b**) δ^{18}O-NO_3^- values in rainwater. The ranges of nitrogen isotopic composition of various NO_x sources and atmospheric NO_3^- are shown, as well as the ranges of oxygen isotopic compositions of O_2, O_3 and atmospheric NO_3^-.

21 % of the catchment area (23.2 kg ha^{-1} yr^{-1}) (Hao et al., 2017). In contrast, the values obtained for dry N deposition in this study were lower than the results reported in the previous study (Hao et al., 2017). The N deposition measured in the present study is lower than in the adjacent capital city of Guizhou province, Guiyang (24.8 kg ha^{-1} yr^{-1}) but there is a lower NH_4^+ component in this urban district (Han et al., 2019; Liu et al., 2017b). Monthly variation in N deposition is related to the amount of precipitation due to precipitation being a primary control of N deposition (Zhang et al., 2008). Monthly DTN deposition rates were positively correlated with the amount of monthly rainfall (R^2 = 0.78, $P < 0.001$ and R^2 = 0.86, $P < 0.001$ for HZV and MZR, respectively), which indicates that the seasonal variation in DTN deposition was controlled by the seasonal variation in rainfall and sources available in the catchment (Liu et al., 2013).

4.2. Sources controlling rainwater inorganic N and nitrate isotopes in karst agriculture

4.2.1. Sources of the NH_4^+–N

The NH_4^+/NO_3^- molar ratio is a good indicator of the relative contributions of agricultural sources (fertilizer and livestock manure) and non-agricultural sources (industrial fossil fuel combustion and vehicle exhaust) to wet N deposition (Zhao et al., 2009). It can provide an indication of the degree of agriculturalization and industrialization on a local scale due to differences between the main sources of NH_4^+ and NO_3^-. As mentioned above, agriculture-associated NH_3 volatilization from fertilizer (urea, di-ammonium phosphate in this study area) and human or animal excrement applied in agricultural soils is the major source of atmospheric NH_4^+ (Zhao et al., 2009). In areas with intensive agricultural production, such as Midwestern USA, Southern Korea and rural China (Fahey et al., 1999; Lee et al., 2012; Zhang et al., 2008), the NH_4^+/NO_3^- molar ratio was greater than 1, while the NH_4^+/NO_3^- molar ratio of rainwater has been reported to be generally lower than 1 in metropolitan areas such as New York (North America), Guangzhou (South China) and Chengdu (Southwest China) (Fahey et al., 1999; Fang et al., 2010; Wang and Han, 2011). In these highly industrialized areas, there are with the approximately equal contributions of NH_4^+ and NO_3^- in rainwater.

In the present study, NH_4^+ contributes significantly more to N deposition than NO_3^-, with the VWM annual NH_4^+/NO_3^- molar ratios higher than 2.0 (Tables S1 and S2), which indicates that agriculture is the predominant source of NH_4^+–N deposition in this catchment. The NH_4^+ in rainwater at the HZV site is more affected by anthropogenic impact, in the form of residential and agricultural land, than at MZR. The lowest NH_4^+/NO_3^- molar ratio was observed in February at both locations (1.5 and 0.9 at HZV and MZR, respectively) indicating that the contribution from agricultural activity to wet N deposition is lower during this month. Using the stable isotopes of wet deposition, one study which has similarly high contributions from NH_4^+–N (~60 %) to annual wet N deposition also concluded that agriculture was a major contributor (Xie et al., 2008).

4.2.2. Source controls of monthly $\delta^{15}N\text{-}NO_3^-$ variation

The dominant oxidation pathways of the nitrate precursor (NO_x) in rainwater have been regarded as a driver of temporal variations in δ^{15}N-NO_3^- values (Freyer et al., 1993; Jarvis et al., 2008). This mechanism explains the variations of δ^{15}N-NO_3^- values in rainwater on the nocturnal and diurnal scale (Freyer et al., 1993). However, the NO_x oxidation pathways seem not to be the reason for the monthly variations of rainwater δ^{15}N-NO_3^- values, which can be proved by the molar ratio of NO_2 and O_3 observed in other studies (Hastings et al., 2003; Elliott et al., 2007). In this study, the monthly NO_2/O_3 shows a similar trend with the isotopic variations and an opposite trend with variations in solar radiation (Fig. S1). However, all the NO_2/O_3 ratios are less than 1 (0.1 to 0.4, Fig. S1), which could not lead to the high δ^{15}N-NO_3^- values via oxidation pathways on the monthly scale. Moreover, since the photochemical oxidation reactions are rapid, the monthly δ^{15}N-NO_3^- values could not be directly applied to explain shorter time variations. Therefore, the NO_x oxidation pathways can only be considered as a potential factor driving the δ^{15}N-NO_3^- seasonal variation in this study. Source variations are therefore the most significant cause of monthly changes in δ^{15}N-NO_3^- values.

Sources of NO_3^- are generally believed to be NO_x emitted from fossil fuel combustion, automobiles, and biomass burning (Zhao et al., 2009), and the NO_x released from the soil by microbial N cycle process (e.g. denitrification). There is a significant difference between the δ^{15}N values of nitrate in rainwater and single NO_x sources, e.g. NO_x emitted from coal combustion (+19.8 ± 5.2‰), vehicle exhaust (−2.5 ± 1.5‰), biomass burning (+12.5 ± 3.1‰), and soil emission (−30.3 ± 9.4‰) (Felix et al., 2013, 2012; Hastings et al., 2009; Li and Wang, 2008; Walters et al., 2015a) (Fig. 3a, Table S3), suggesting that there is mixing of nitrate from these sources and temporal changes in contributions from different sources (see section 4.3).

Although the monthly δ^{15}N-NO_3^- values are close to δ^{15}N-NO_x values of vehicle exhaust (Walters et al., 2015a) (Fig. 3a), it cannot be concluded that the seasonal variation in δ^{15}N-NO_3^- is controlled by the nitrate derived from vehicle exhaust, as the study area is located in a rural region and NO_x emissions from vehicle exhaust is not likely to vary seasonally.

The negative δ^{15}N-NO_3^- values in summer rainwater observed in this study (Fig. 3a) are similar to the results of other studies (Chen et al., 2019; Fang et al., 2010; Zhang et al., 2008). This represents the main period of fertilizer application to crops. Additionally, the higher temperatures in summer could accelerate NO_x production via agricultural soil microbial N cycle processes (e.g. nitrification/denitrification). Soil microorganisms can convert organic nitrogen (e.g. urea and manure)

used in agricultural production into NO_3^- following Eq. (1). Meanwhile, these microorganisms can also denitrify NO_3^- into NO_x according to Eq. (2) and subsequently release N to the atmosphere (Chen et al., 2019; Felix et al., 2012; Lee et al., 2012).

$$ON \rightarrow NH_4^+ \rightarrow NO_2^- \rightarrow NO_3^- \quad (1)$$

$$NO_3^- \rightarrow NO_2^- \rightarrow NO \rightarrow N_2O \quad (2)$$

Due to such processes, the heavy and frequent rainfall in June and July may capture the emissions of ^{15}N-depleted NO_x microorganism denitrification of agricultural soil (Elliott et al., 2019; Felix et al., 2013; Wang et al., 2018). This suggests that more NO_3^- during this time period should originate from soil emissions via chemical N fertilizer application and the subsequently microbial N cycle. After the intensive fertilization period, nitrogen availability gradually decreases and subsequently the NO_x emission from farmland decline.

It should be noted that δ^{15}N-NO_x values from biomass burning are more positive than the δ^{15}N-NO_3^- in rainwater (Felix et al., 2012; Hastings et al., 2009) (Fig. 3a), which may result in a secondary peak in the δ^{15}N-NO_3^- values of rainwater in September and November due to the agricultural practice of burning more straw during these months. The increase in δ^{15}N-NO_3^- values until February suggest contribution from soil emissions gradually decreases, or that there is an increased contribution from other sources with high δ^{15}N values, such as coal combustion (Fig. 3a) (Felix et al., 2012). Previous studies have found that the seasonal proportions of NO_x emissions from cultivated land in China were 20.9 %, 75.8 %, 2.6 % and 0.7 % in spring, summer, autumn and winter, respectively (Xie et al., 2005), and a similar seasonal trend has been reported in the United States (Williams et al., 1992).

Although electricity production from thermal power by coal combustion is non-seasonal, this process releases significant NO_x to the atmosphere that can be transported long-distances to the catchment (Zeng et al., 2019), which results in the contribution from this source being higher during autumn and winter due to the reduction in soil NO_x emissions (the reduction in agricultural fertilization). In the study catchment, there is substantial seasonal variation in coal combustion for heating requirements. Residents burn significantly more coal in winter, which could be the cause of increased δ^{15}N-NO_3^- values due to increased NO_x formation (Yeon et al., 2015).

4.2.3. Monthly variation of δ^{18}O-NO_3^-

As shown in Fig. 3b, most rainwater oxygen isotope values from October to May were higher than 60‰, while the rainwater samples in summer and early fall had lower δ^{18}O-NO_3^- values in summer and early fall were relatively close to the signatures of $\delta^{18}O_2$ (+23.5‰) (Kendall et al., 2007). Monthly variation in δ^{18}O-NO_3^- values was similar to δ^{15}N-NO_3^-, which has been widely observed (Hastings et al., 2003; Yeon et al., 2015). In winter, weak solar radiation (Fig. S1) and reduced photochemical activity means nitrates are produced primarily by the N_2O_5-radical pathway (the production of HNO_3 via the N_2O_5 pathway), resulting in increasing δ^{18}O-NO_3^- values (Fang et al., 2010; Hastings et al., 2003). However, during the summer, strong solar radiation enhances the OH-radical pathway producing decreased δ^{18}O-NO_3^- values (Hastings et al., 2003). Moreover, the δ^{18}O-NO_x from coal combustion and vehicle exhaust may be close to the $\delta^{18}O_2$ of the atmosphere (Kendall et al., 2007), due to the chemical reaction with nitrogen species and atmospheric oxygen in these emission processes, which is not likely to vary seasonally. Additionally, during denitrification (soil microbial N cycle processes), the δ^{15}N and δ^{18}O values will increase simultaneously in the residual nitrate, resulting in a negative δ^{18}O value occurring in the production of NO_x, while the δ^{18}O-NO_3^- values in our rainwater samples are extremely positive (Fig. 3b, Tables S1 and S2). Therefore, the results of this study suggest that δ^{18}O-NO_3^- values in rainwater, and their variation, are primarily controlled by the atmospheric cycle of nitrates and show the δ^{18}O signature of photochemical reactants like O_3 ($\delta^{18}O_3$ = +90‰ to +122‰) (Johnston and Thiemens, 1997; Kendall et al., 2007).

4.3. Source contributions to nitrate in rainfall based on SIAR model

Although it is well established that major seasonal sources contributor to the rainwater nitrate, the contributions from each source are still unquantified. Previous studies have used the SIAR model to calculate source contributions based on two conditions: (i) δ^{15}N values of primary NO_x emissions are distinct, and (ii) rainfall washes down both gaseous and particulate N species efficiently (Liu et al., 2017b). In the last decade, there has been significant work measuring the typical δ^{15}N values of NO_x emissions from different sources (Table S3), which can be used to calculate source contributions. We considered the contribution from lightning NO_x (δ^{15}N= −0.5‰–1.4‰) (Liu et al., 2017b) is negligible because the more negative values of δ^{15}N-NO_3^- occur in May to August, when lightning occurs with a high frequency. However, since there is insufficient knowledge of the δ^{18}O values of atmospheric NO_x, δ^{18}O values were not adopted in source apportionment for sources controlled by the complex photochemical reaction processes of NO_x emissions with oxidants (e.g. ozone).

N isotope equilibrium exchange fractionation (> 34‰, depending on experimental conditions) would occur during the NO-NO_2 cycle, and result in ^{15}N enrichment in more oxidized forms that is subsequently oxidized to NO_3^- in rainwater (Heaton et al., 1997; Walters et al., 2015b). In this scenario, if rainwater NO_3^- (ranging from −9.1 ‰ to +2.5 ‰) was produced by ^{15}N-enriched NO_2 via the NO-NO_2 cycle in our study, the expected δ^{15}N values of primary NO_x emissions would be −43.1‰to −31.5‰ (considering the minimum isotopic exchange equilibrium of 34‰), which could not explained by δ^{15}N values of major NO_x emission sources (−30.3‰ to +19.8‰ on average; Table S3). Additionally, previous studies have found that the impact of nitrate isotope washout might be less important on seasonal timescales (Chen et al., 2019). In this study, there was no clear relationship between rainfall and δ^{15}N-NO_3^- values of rainwater (R^2 = −0.36, $P < 0.01$, HZV; R^2 = −0.17, MZR), suggesting rainfall is not a strong influence on δ^{15}N-NO_3^-. Consequently, we assumed that the difference in δ^{15}N values between NO_x emission sources and rainwater NO_3^- is negligible, which is also assumed in other studies (Elliott et al., 2015; Liu et al., 2017b; Morin et al., 2009).

Although the mean proportional contribution of different sources will be slightly potential biases due to this assumption, the annual mean probability estimate (AMPE) within 95 % credible interval and the relative difference of proportional contribution of different sources are acceptable (Liu et al., 2017b). Using δ^{15}N-NO_x values of different sources (Table S3) and the δ^{15}N-NO_3^- values of rainwater (Table S4), the contribution of major NO_x sources to rainwater nitrate was estimated using the SIAR model (Fig. 4). The modeling results showed that NO_x from coal combustion, vehicle exhaust, biomass burning, and soil emissions accounted for 20.0 %, 25.6 %, 22.9 % and 31.5 % respectively (AMPE) in rainwater NO_3^- at HZV, and 19.0 %, 27.8 %, 23.2 % and 30.0 % (AMPE) in rainwater NO_3^- at MZR (Fig. 4a, b, c, and d). Compared with the contribution rate of rainwater NO_3^- collected in a karst urban area (Liu et al., 2017b), soil emission by microbial N cycle processes substantially influenced δ^{15}N-NO_3^- signatures and was the primary contributor to NO_3^- in rainwater of the karst agricultural catchment, particularly during the growing season (Fig. 4d), while the vehicle exhaust contribution was stable as the secondary contributor (Fig. 4b). This relatively high contribution from vehicle exhaust is unlikely to be from a local source as there are few vehicles in this agricultural catchment. The most likely explanation is that the vehicle exhaust is from surrounding cites. Comparing the results from this study with a karst urban area (Guiyang) (Liu et al., 2017b), there was no significant difference in the contributions of NO_x from coal combustion and biomass burning. Moreover, the contributions of coal combustion and biomass burning were lower in warm months and higher in cold months, while soil emission showed the opposite trend (Fig. 4a, c, and

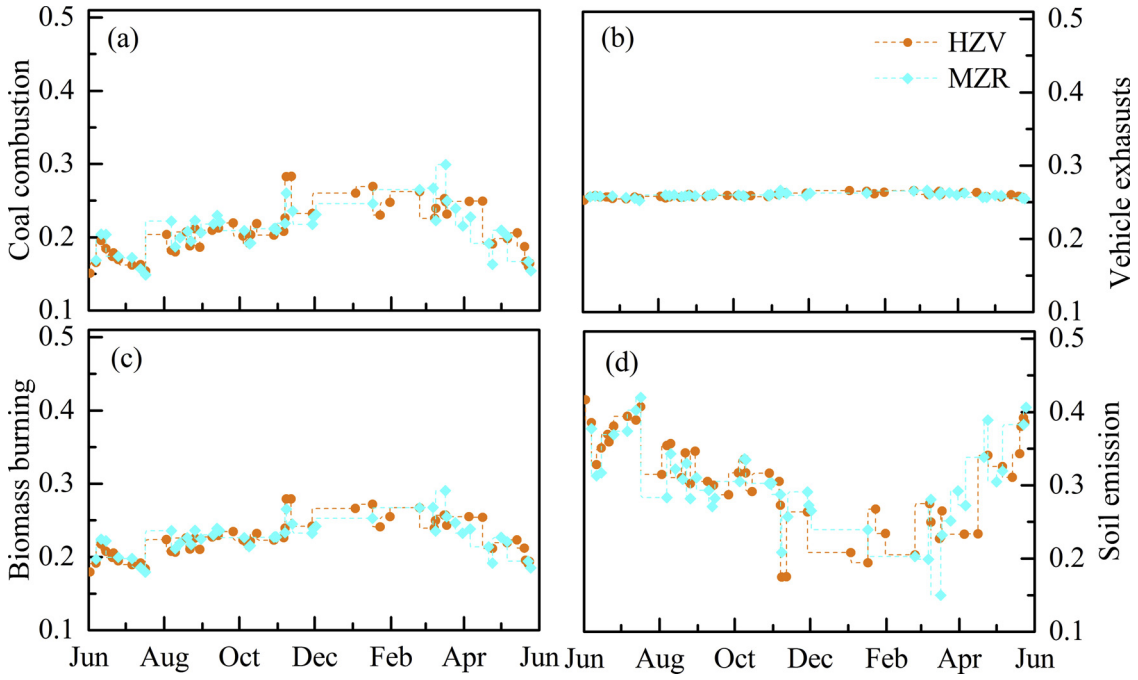

Fig. 4. Mean proportional contribution of major NO_x sources to NO_3^- in precipitation at HZV and MZR as calculated by SIAR.

d).

The source contribution calculation demonstrates that agricultural activity is a strong driver of the NO_3^- in rainwater via soil emissions contribution. These results also indicate that excess fertilization is prevalent in karst agricultural areas, which could significantly influence the atmospheric wet nitrogen deposition and further impact the agricultural ecosystems. The low efficiency of fertilization of farmland is a matter for concern because of the critical link to the karst N cycle. The efficiency of agricultural fertilization therefore needs to be improved to promote higher quality agricultural eco-environmental management (Oliver et al., 2020).

4.4. Spatial variations of nitrate isotopic composition and nitrate isotopes in different climatic zones

The annual mean $\delta^{15}N\text{-}NO_3^-$ value was slightly more negative in HZV (-2.8‰) than at MZR (-2.7‰). Moreover, there are more months when HZV has lower $\delta^{15}N\text{-}NO_3^-$ values (June, August, September, February, March, and May) than MZR (Fig. 5). For $\delta^{18}O\text{-}NO_3^-$, the annual mean values were slightly higher in HZV (+66.9‰) than in MZR (+65.9‰). But lower $\delta^{18}O\text{-}NO_3^-$ values were still observed at

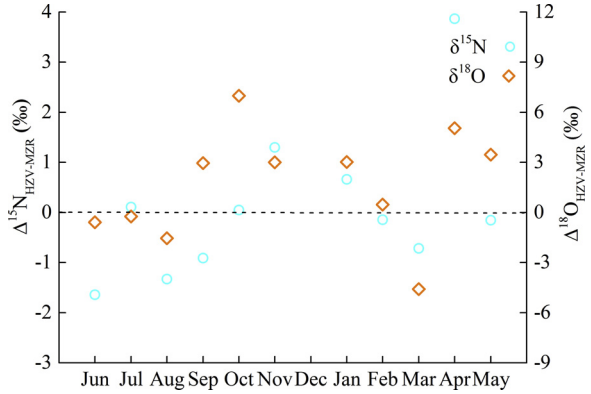

Fig. 5. Differences in nitrogen ($\Delta^{15}N_{HZV\text{-}MZR}$) and oxygen ($\Delta^{18}O_{HZV\text{-}MZR}$) isotopic composition of precipitation nitrates.

HZV than MZR for several months (June, July, August, and March). Dual isotopes of nitrate were consistently lower at HZV than MZR for three months (June, August, and March) and HZV in four months (October, November, January, and April) were higher than MZR (Fig. 5).

This type of monthly nitrate isotopic differences in rainwater on small catchment scales has not been reported in previous studies. In the current study, the spatial variation may depend on the particulate deposition process, sources, and photochemical reactions occurring at each site. For example, one study in USA suggested that dry deposition (HNO_3 (g) and particulate NO_3^-) had consistently higher $\delta^{15}N$ values than wet deposition (NO_3^-) while the $\delta^{18}O$ values are also higher in dry deposition but not as pronounced as $\delta^{15}N$ (Elliott et al., 2015). The $\delta^{15}N\text{-}NO_3^-$ and $\delta^{18}O\text{-}NO_3^-$ values at HZV during October, November, January, and April were consistently higher than at MZR, indicating HZV was more affected by particulates with its higher dual isotopic values during these months, while MZR was more affected by particulates in June, August, and March (Fig. 5). Additionally, the spatial variation in land use and topography can also impact the source flux and photochemical reactions which result in the spatial variation of NO_x among two sites. The possible fractionation in the diffusion process of NO_x from different sources in the atmosphere may also affect spatial variation. To further investigate the controls on dry and wet deposition, further measurements such as the dual isotopic composition of dry deposition and NO_x levels are required.

Comparing to other studies in different climatic zones, NO_3^-–N concentrations of our study area (0.3 mg L^{-1}) are within the ranges of those reported in the literature for different climatic zones (0.1–1.2 mg L^{-1}) (Table 1). In subtropical climatic zones, NO_3^-–N concentrations in this study are closer to those observed in rural areas and oceanic islands but lower than cities in karst regions and metropolitan areas more generally (Altieri et al., 2013; Fang et al., 2010; Lee et al., 2012; Liu et al., 2017b).

We further compared the $\delta^{15}N\text{-}NO_3^-$ values with all those studies in subtropical climatic regions (Table 1). The results in this study are more negative than in a nearby karst city (Guiyang), a coastal city (Guangzhou), and a metropolitan area close to rural areas in South Korea, but more similar to those obtained in a study on an oceanic island (Bermuda island) (Altieri et al., 2013; Fang et al., 2010; Lee

Table 1
Comparison of NO_3^-–N concentration and dual isotopes in rainwater of Houzhai Catchment with those reported in the literature for different climatic zones.

Study site	N (mg/L)	$\delta^{15}N$ (‰)	$\delta^{18}O$ (‰)	Climatic	Types	Reference
HZV [a]	0.3	−2.8	66.9	SCMC	Rural	This study
MZR [a]	0.3	−2.7	65.9	SCMC	Rural	This study
Guiyang [a]	0.5	−1.4	ND	SCMC	City	Liu et al., 2017b
Guangzhou [a]	1.0	3.0	66.5	SOMC	Metropolis	Fang et al., 2010
Bermuda island [b]	0.1	−2.6	71.1	SOMC	Island	Altieri et al., 2013
South Korea in 2007 [a]	0.1	1.5	ND	SOMC	City close to rural	Lee et al., 2012
South Korea in 2008 [a]	0.2	−0.5	ND	SOMC	City close to rural	Lee et al., 2012
Ochang, South Korea [a]	0.4	5.2	75.9	TOMC	Suburban forests	Yeon et al., 2015
Beijing [b]	ND	−6.8	ND	TCMC	Metropolis	Zhang et al., 2008
Sapporo (Japan) [c]	ND	−4.7–3.4	ND	TCMC	City	Nelson et al., 2018
Rishiri island (Japan) [c]	ND	−8.6–2.0	ND	TCMC	Island	Nelson et al., 2018
Sault Ste (Canada) [b]	0.4	−6.2	54.9	TCMC	City	Spoelstra et al., 2004
Hamburg (Germany) [a]	ND	0.1	ND	TOMC	Forest & grassland	Beyn et al., 2014
Zhanjiang (China) [a]	0.2	0.8	52.4	TRMC	City	Chen et al., 2019
Mediterranean Sea [b]	ND	−4.3	ND	MC	Rural	Mara et al., 2009

[a] Volume-weighted mean for NO_3^--N Concentration and numerical mean for nitrate isotopes.
[b] Numerical mean (mean ± SD).
[c] Range (minimum ~ maximum); ND, no data; SCMC, subtropical continental monsoonal climate; SOMC, subtropical oceanic monsoonal climate; TOMC, temperate oceanic monsoonal climate; TCMC, temperate continental monsoonal climate; TRMC, tropical monsoon climate; MC, Mediterranean climate.

et al., 2012; Liu et al., 2017b). This illustrates that the $\delta^{15}N$-NO_3^- values from sites in a similar climatic zone are strongly influenced by emissions from human activity in urban areas (e.g. coal combustion, producing higher isotope values). Moreover, the $\delta^{15}N$-NO_3^- values in rainwater in our study seemed to be higher than those in most temperate regions (Beijing, Sapporo, Rishiri island, North of Sault Ste), except in temperate forest areas (Ochang, Hamburg) (Beyn et al., 2014; Nelson et al., 2018; Spoelstra et al., 2004; Yeon et al., 2015; Zhang et al., 2008), and also higher than monitoring data from a site in the eastern Mediterranean Sea (representing a Mediterranean climate site) (Mara et al., 2009). Compared with a tropical industrial city, the $\delta^{15}N$-NO_3^- values in this study are also negative (Chen et al., 2019), while our $\delta^{18}O$-NO_3^- values for rainwater are similar to those obtained in subtropical urban areas (Guangzhou), and lower than the subtropical oceanic island (Bermuda island), but much higher than temperate regions (North of Sault Ste) and a tropical industrial city (Zhanjiang) (Altieri et al., 2013; Chen et al., 2019; Fang et al., 2010; Spoelstra et al., 2004). Overall, the dual isotopic composition of rainwater in different climatic zone varies greatly and is strongly affected by the local environment (e.g. agricultural activities in present study).

5. Conclusions

This study aims to explore the nitrogen wet deposition process, identify the factors controlling spatial-temporal variations, and quantify the contribution of different sources to rainwater nitrate in a typical karst agricultural catchment, located in the center of one of three world's largest continuous karst areas. Base on the N chemical and NO_3^- isotope geochemistry of one-year rainwater samples, the relatively high nitrogen deposition rate (21.8 and 17.1 kg ha^{-1} yr^{-1} at HZV and MZR, respectively) compared to the Chinese average value were observed. In combined with the Bayesian isotope mixing model and dual isotopes, here we concluded that agriculture is the driver of nitrogen wet deposition process. Particularly, the nitrogen emission (e.g. NO_x and NH_3) from farmland controlled the seasonal variations in nitrogen deposition process and nitrate isotopes. Moreover, the SIAR model result quantifies the contributions of major sources to rainwater NO_3^-. That is, soil emission processes within the microbial N cycle (31.5 %), and vehicle exhaust (25.6 %), were the first and second largest contributors, which drove the NO_3^- in rainwater. These results highlight the importance of agricultural activity as a driver of nitrogen wet deposition in agricultural catchment regions.

Declaration of Competing Interest

The authors declare no competing financial interest.

Acknowledgements

This work was supported by the National Natural Science Foundation of China [grant number 41571130072, 41925002]; the National Key R&D Program of China [grant number 2016YFA0601002]; the UK Natural Environment Research Council [grant number NE/N007395/1]; and the Independent Innovative Foundation of Tianjin University [grant number 2019XZS-0016].

Appendix A. Supplementary data

Supplementary material related to this article can be found, in the online version, at doi:https://doi.org/10.1016/j.agee.2020.106883.

References

Altieri, K.E., Hastings, M.G., Gobel, A.R., Peters, A.J., Sigman, D.M., 2013. Isotopic composition of rainwater nitrate at Bermuda: the influence of air mass source and chemistry in the marine boundary layer. J. Geophys. Res. Atmos. 118 11-11, 316.
Beyn, F., Matthias, V., Dähnke, K., 2014. Changes in atmospheric nitrate deposition in Germany—An isotopic perspective. Environ. Pollut. 194, 1–10.
Bobbink, R., Hicks, K., Galloway, J., Spranger, T., Alkemade, R., Ashmore, M., Bustamante, M., Cinderby, S., Davidson, E., Dentener, F., Emmett, B., Erisman, J.W., Fenn, M., Gilliam, F., Nordin, A., Pardo, L., De Vries, W., 2010. Global assessment of nitrogen deposition effects on terrestrial plant diversity: a synthesis. Ecol. Appl. 20, 30–59.
Chang, Y.H., Zhang, Y.L., Tian, C.G., Zhang, S.C., Ma, X.Y., Cao, F., Liu, X.Y., Zhang, W.Q., Kuhn, T., Lehmann, M.F., 2018. Nitrogen isotope fractionation during gas-to-particle conversion of NOx to NO3- in the atmosphere – implications for isotope-based NOx source apportionment. Atmos. Chem. Phys. 18, 11647–11661.
Chen, X.Y., Mulder, J., 2007. Atmospheric deposition of nitrogen at five subtropical forested sites in South China. Sci. Total Environ. 378, 317–330.
Chen, X., Chen, C., Hao, Q., Zhang, Z., Shi, P., 2008. Simulation of rainfall-underground outflow responses of a karstic watershed in Southwest China with an artificial neural network. Water Sci. Eng. 1, 1–9.
Chen, F., Lao, Q., Jia, G., Chen, C., Zhu, Q., Zhou, X., 2019. Seasonal variations of nitrate dual isotopes in wet deposition in a tropical city in China. Atmos. Environ. 196, 1–9.
Elliott, E.M., Kendall, C., Wankel, S.D., Burns, D.A., Boyer, E.W., Harlin, K., Bain, D.J., Butler, T.J., 2007. Nitrogen isotopes as indicators of NO(x) source contributions to atmospheric nitrate deposition across the midwestern and northeastern United States. Environ. Sci. Technol. 41, 7661–7667.
Elliott, E.M., Kendall, C., Boyer, E.W., Burns, D.A., Lear, G.G., Golden, H.E., Harlin, K., Bytnerowicz, A., Butler, T.J., Glatz, R., 2015. Dual nitrate isotopes in dry deposition: utility for partitioning NOx source contributions to landscape nitrogen deposition. J. Geophys. Res. Biogeosci. 114, 425–453.
Elliott, E.M., Yu, Z., Cole, A.S., Coughlin, J.G., 2019. Isotopic advances in understanding

reactive nitrogen deposition and atmospheric processing. Sci. Total Environ. 662, 393–403.
Erisman, J.W., Bleeker, A., Galloway, J., Sutton, M.S., 2007. Reduced nitrogen in ecology and the environment. Environ. Pollut. 150, 140–149.
Fahey, T.J., Williams, C.J., Rooneyvarga, J.N., Cleveland, C.C., Postek, K.M., Smith, S.D., Bouldin, D.R., 1999. Nitrogen deposition in and around an intensive agricultural district in central New York. J. Environ. Qual. 28, 1585–1600.
Fang, Y.T., Koba, K., Wang, X.M., Wen, D.Z., Li, J., Takebayashi, Y., Liu, X.Y., Yoh, M., 2010. Anthropogenic imprints on nitrogen and oxygen isotopic composition of precipitation nitrate in a nitrogen-polluted city in southern China. Atmos. Chem. Phys. 10, 1313–1325.
Felix, J.D., Elliott, E.M., Shaw, S.L., 2012. Nitrogen isotopic composition of coal-fired power plant NOx: influence of emission controls and implications for global emission inventories. Environ. Sci. Technol. 46, 3528.
Felix, J.D., Elliott, E.M., Gish, T.J., Mcconnell, L.L., Shaw, S.L., 2013. Characterizing the isotopic composition of atmospheric ammonia emission sources using passive samplers and a combined oxidation-bacterial denitrifier approach. Rapid Commun. Mass Spectrom. 27, 2239–2246.
Fibiger, D.L., Hastings, M.G., 2016. First measurements of the nitrogen isotopic composition of NOx from biomass burning. Environ. Sci. Technol. 50, 11569–11574.
Freyer, H.D., Kley, D., Volz-Thomas, A., Kobel, K., 1993. On the interaction of isotopic exchange processes with photochemical reactions in atmospheric oxides of nitrogen. J. Geophys. Res. Atmos. 98, 14791–14796.
Galloway, J.N., Townsend, A.R., Erisman, J.W., Bekunda, M., Cai, Z., Freney, J.R., Martinelli, L.A., Seitzinger, S.P., Sutton, M.A., 2008. Transformation of the nitrogen cycle: recent trends, questions, and potential solutions. Science 320, 889.
Gao, Y., Zhou, F., Ciais, P., Miao, C., Yang, T., Jia, Y., Zhou, X., Klaus, B.-B., Yu, G., Yang, T., 2019. Human activities aggravate nitrogen deposition pollution to inland water over china. Sci. Rev. https://doi.org/10.1093/nsr/nwz073.
Hall, S.J., Ogata, E.M., Weintraub, S.R., Baker, M.A., Ehleringer, J.R., Czimczik, C.I., Bowling, D.R., 2016. Convergence in nitrogen deposition and cryptic isotopic variation across urban and agricultural valleys in northern Utah. J. Geophys. Res. Biogeosci. 121, 2340–2355.
Han, G., Song, Z., Tang, Y., Wu, Q., Wang, Z., 2019. Ca and Sr isotope compositions of rainwater from Guiyang city, Southwest China: Implication for the sources of atmospheric aerosols and their seasonal variations. Atmos. Environ. 214, 116854.
Hao, Z., Gao, Y., Yang, T.T., Tian, J., 2017. Atmospheric wet deposition of nitrogen in a subtropical watershed in China: characteristics of and impacts on surface water quality. Environ. Sci. Pollut. R. 24, 8489–8503.
Hastings, M.G., Sigman, D.M., Lipschultz, F., 2003. Isotopic evidence for source changes of nitrate in rain at Bermuda. J. Geophys. Res. Atmos. 108, 4790.
Hastings, M.G., Jarvis, J.C., Steig, E.J., 2009. Anthropogenic impacts on nitrogen isotopes of ice-core nitrate. Science 324 1288–1288.
Heaton, T.H.E., Spiro, B., Robertson, S.M.C., 1997. Potential canopy influences on the isotopic composition of nitrogen and sulphur in atmospheric deposition. Oecologia 109, 600–607.
IUSS Working Group WRB, 2015. World Reference Base for Soil Resources 2014, Update 2015 International Soil Classification System for Naming Soils and Creating Legends for Soil Maps. World Soil Resources Reports No. 106. FAO, Roma IT EU, pp. 192.
Jang, M.S., Kamens, R.M., 2001. Characterization of secondary aerosol from the photooxidation of toluene in the presence of NOx and 1-propene. Environ. Sci. Technol. 35, 3626–3639.
Jarvis, J.C., Steig, E.J., Hastings, M.G., Kunasek, S.A., 2008. Influence of local photochemistry on isotopes of nitrate in Greenland snow. Geophys. Res. Lett. 35, L21804.
Jin, Z., Zheng, Q., Zhu, C., Wang, Y., Cen, J., Li, F., 2018. Contribution of nitrate sources in surface water in multiple land use areas by combining isotopes and a Bayesian isotope mixing model. Appl. Geochem. 93, 10–19.
Jin, Z., Wang, Y., Qian, L., Hu, Y., Jin, X., Hong, C., Li, F., 2019. Combining chemical components with stable isotopes to determine nitrate sources of precipitation in Hangzhou and Huzhou, SE China. Atmos. Pollut. Res. 10, 386–394.
Johnston, J.C., Thiemens, M.H., 1997. The isotopic composition of tropospheric ozone in three environments. J. Geophys. Res. 102, 25395–25404.
Kawashima, H., Kurahashi, T., 2011. Inorganic ion and nitrogen isotopic compositions of atmospheric aerosols at Yurihonjo, Japan: implications for nitrogen sources. Atmos. Environ. 45, 6309–6316.
Kendall, C., Elliott, E.M., Wankel, S.D., 2007. Tracing Anthropogenic Inputs of Nitrogen to Ecosystems. Blackwell Publishing Ltd.
Lee, K.-S., Lee, D.-S., Lim, S.-S., Kwak, J.-H., Jeon, B.-J., Lee, S.-I., Lee, S.-M., Choi, W.-J., 2012. Nitrogen isotope ratios of dissolved organic nitrogen in wet precipitation in a metropolis surrounded by agricultural areas in southern Korea. Agric. Ecosyst. Environ. 159, 161–169.
Li, D., Wang, X., 2008. Nitrogen isotopic signature of soil-released nitric oxide (NO) after fertilizer application. Atmos. Environ. 42, 4747–4754.
Li, C., Li, S.-L., Yue, F.-J., He, S.-N., Shi, Z.-B., Di, C.-L., Liu, C.-Q., 2020. Nitrate sources and formation of rainwater constrained by dual isotopes in Southeast Asia: example from Singapore. Chemosphere 241, 125024.
Liu, X., Zhang, Y., Han, W., Tang, A., Shen, J., Cui, Z., Vitousek, P., Erisman, J.W., Goulding, K., Christie, P., 2013. Enhanced nitrogen deposition over China. Nature 494, 459.
Liu, C., Liu, Y., Guo, K., Wang, S., Liu, H., Zhao, H., Qiao, X., Hou, D., Li, S., 2016. Aboveground carbon stock, allocation and sequestration potential during vegetation recovery in the karst region of southwestern China: a case study at a watershed scale. Agric. Ecosyst. Environ. 235, 91–100.
Liu, X., Xu, W., Duan, L., Du, E., Pan, Y., Lu, X., Zhang, L., Wu, Z., Wang, X., Zhang, Y., Shen, J., Song, L., Feng, Z., Liu, X., Song, W., Tang, A., Zhang, Y., Zhang, X., Collett, J.L., 2017a. Atmospheric nitrogen emission, deposition, and air quality impacts in China: an overview. Curr. Pollut. Rep. 3, 65–77.
Liu, X.Y., Xiao, H.W., Xiao, H.Y., Song, W., Sun, X.C., Zheng, X.D., Liu, C.Q., Koba, K., 2017b. Stable isotope analyses of precipitation nitrogen sources in Guiyang, southwestern China. Environ. Pollut. 230, 486.
Liu, M., Han, G., Zhang, Q., 2020. Effects of agricultural abandonment on soil aggregation, soil organic carbon storage and stabilization: results from observation in a small karst catchment, Southwest China. Agric. Ecosyst. Environ. 288, 106719.
Lü, P., Han, G., Wu, Q., 2017. Chemical characteristics of rainwater in karst rural areas, Guizhou Province, Southwest China. Acta Geochim. 36, 572–576.
Mara, P., Mihalopoulos, N., Gogou, A., Daehnke, K., Schlarbaum, T., Emeis, K.C., Krom, M., 2009. Isotopic composition of nitrate in wet and dry atmospheric deposition on Crete in the eastern Mediterranean Sea. Glob. Biogeochem. Cycles 23.
Mcilvin, M.R., Casciotti, K.L., 2011. Technical updates to the bacterial method for nitrate isotopic analyses. Anal. Chem. 83, 1850–1856.
Moore, J.W., Semmens, B.X., 2008. Incorporating uncertainty and prior information into stable isotope mixing models. Ecol. Lett. 11, 470–480.
Morin, S., Savarino, J., Frey, M.M., Domine, F., Jacobi, H.W., Kaleschke, L., Martins, J.M.F., 2009. Comprehensive isotopic composition of atmospheric nitrate in the Atlantic Ocean boundary layer from 65°S to 79°N. J. Geophys. Res. Atmos. 114.
Nelson, D.M., Tsunogai, U., Dong, D., Ohyama, T., Komatsu, D.D., Nakagawa, F., Noguchi, I., Yamaguchi, T., 2018. Triple oxygen isotopes indicate urbanization affects sources of nitrate in wet and dry atmospheric deposition. Atmos. Chem. Phys. 1–30.
Oliver, D.M., Zheng, Y., Naylor, L.A., Murtagh, M., Waldron, S., Peng, T., 2020. How does smallholder farming practice and environmental awareness vary across village communities in the karst terrain of southwest China? Agricult. Ecosyst. Environ. 288, 106715.
Parnell, A.C., Inger, R., Bearhop, S., Jackson, A.L., 2010. Source partitioning using stable isotopes: coping with too much variation. PLoS One 5, e9672.
Qin, C., Li, S.-L., Yue, F.-J., Xu, S., Ding, H., 2019. Spatiotemporal variations of dissolved inorganic carbon and controlling factors in a small karstic catchment, Southwestern China. Earth Surf. Process. Landf. 44, 2423–2436.
Spoelstra, J., Schiff, S.L., Jeffries, D.S., Semkin, R.G., 2004. Effect of storage on the isotopic composition of nitrate in bulk precipitation. Environ. Sci. Technol. 38, 4723–4727.
Stock, B.C., Semmens, B.X., 2016. Unifying error structures in commonly used biotracer mixing models. Ecology 97, 2562–2569.
Walters, W.W., Goodwin, S.R., Michalski, G., 2015a. Nitrogen stable isotope composition (δ15N) of vehicle-emitted NOx. Environ. Sci. Technol. 49, 2278–2285.
Walters, W.W., Simonini, D.S., Michalski, G., 2015b. Nitrogen isotope exchange between NO and NO2 and its implications for δ15N variations in tropospheric NOx and atmospheric nitrate. Geophys. Res. Lett. 43, 440–448.
Wang, H., Han, G., 2011. Chemical composition of rainwater and anthropogenic influences in Chengdu, Southwest China. Atmos. Res. 99, 190–196.
Wang, Z.J., Yue, F.J., Li, S.L., Li, X.D., Wang, S.L., Li, C., Tao, F.X., 2018. Nitrate dynamics during impoundment and flood periods in a subtropical karst reservoir: Hongfeng Lake, Southwestern China. Environ. Sci. Proces. Impacts 20, 1736–1745.
Wang, Z.-J., Li, S.-L., Yue, F.-J., Qin, C.-Q., Buckerfield, S., Zeng, J., 2020. Rainfall driven nitrate transport in agricultural 1 karst surface river system: insight from high resolution hydrochemistry and nitrate isotopes. Agric. Ecosyst. Environ. 291, 106787.
Wei, J., Huang, W., Li, Z., Xue, W., Peng, Y., Sun, L., Cribb, M., 2019a. Estimating 1-km-resolution PM2.5 concentrations across China using the space-time random forest approach. Remote Sens. Environ. 231, 111221.
Wei, J., Li, Z., Guo, J., Sun, L., Huang, W., Xue, W., Fan, T., Cribb, M., 2019b. Satellite-Derived 1-km-Resolution PM1 Concentrations from 2014 to 2018 across China. Environ. Sci. Technol. 53, 13265–13274.
Williams, E.J., Guenther, A., Fehsenfeldi, F.C., 1992. An inventory of nitric oxide emissions from soils in the United States. J. Geophys. Res. Atmos. 97, 7511–7519.
Wu, Q., Han, G., Tao, F., Tang, Y., 2012. Chemical composition of rainwater in a karstic agricultural area, Southwest China: the impact of urbanization. Atmos. Res. 111, 71–78.
Xiao, H.W., Xiao, H.Y., Long, A.M., Wang, Y.L., 2012. Who controls the monthly variations of NH4+ nitrogen isotope composition in precipitation? Atmos. Environ. 54, 201–206.
Xie, M., Wang, T., Zhang, M., Yang, X., 2005. Modeling of NOx emissions from soil and their effect on tropospheric photochemistry in China. Acta Pedol. Sin. 42, 948–956 (in Chinese).
Xie, Y.X., Xiong, Z.Q., Xing, G.X., Yan, X.Y., Shi, S.L., Sun, G.Q., Zhu, Z.L., 2008. Source of nitrogen in wet deposition to a rice agroecosystem at Tai lake region. Atmos. Environ. 42, 5182–5192.
Yeon, J., Gautam, M.K., Kim, I., Lee, S., Lee, D., An, H.J., Lees, K.S., 2015. Isotopic composition of throughfall nitrates in suburban forests with different vegetations. Geosci. J. 19, 167–175.
Yu, G., Jia, Y., He, N., Zhu, J., Chen, Z., Wang, Q., Piao, S., Liu, X., He, H., Guo, X., Wen, Z., Li, P., Ding, G., Goulding, K., 2019. Stabilization of atmospheric nitrogen deposition in China over the past decade. Nat. Geosci. 12, 424–429.
Yue, F.J., Li, S.L., Liu, C.Q., Lang, Y.C., Ding, H., 2015. Sources and transport of nitrate constrained by the isotopic technique in a karst catchment: an example from Southwest China. Hydrol. Process. 29, 1883–1893.
Yue, F.-J., Waldron, S., Li, S.-L., Wang, Z.-J., Zeng, J., Xu, S., Zhang, Z.-C., Oliver, D.M., 2019. Land use interacts with changes in catchment hydrology to generate chronic nitrate pollution in karst waters and strong seasonality in excess nitrate export. Sci. Total Environ. 696, 134062.
Zeng, J., Yue, F.-J., Wang, Z.-J., Wu, Q., Qin, C.-Q., Li, S.-L., 2019. Quantifying depression trapping effect on rainwater chemical composition during the rainy season in karst agricultural area, southwestern China. Atmos. Environ. 218, 116998.

Zeng, J., Han, G., Wu, Q., Tang, Y., 2020. Effects of agricultural alkaline substances on reducing the rainwater acidification: insight from chemical compositions and calcium isotopes in a karst forests area. Agric. Ecosyst. Environ. 290, 106782.
Zhang, Y., Liu, X.J., Fangmeier, A., Goulding, K.T.W., Zhang, F.S., 2008. Nitrogen inputs and isotopes in precipitation in the North China Plain. Atmos. Environ. 42, 1436–1448.
Zhang, Z., Chen, X., Soulsby, C., 2017. Catchment-scale conceptual modelling of water and solute transport in the dual flow system of the karst critical zone. Hydrol. Process. 31, 3421–3436.
Zhao, X., Yan, X., Xiong, Z., Xie, Y., Xing, G., Shi, S., Zhu, Z., 2009. Spatial and temporal variation of inorganic nitrogen wet deposition to the Yangtze River delta region, China. Water, Air, Soil Pollut. 203, 277–289.
Zhu, J.X., He, N.P., Wang, Q.F., Yuan, G.F., Wen, D., Yu, G.R., Jia, Y.L., 2015. The composition, spatial patterns, and influencing factors of atmospheric wet nitrogen deposition in Chinese terrestrial ecosystems. Sci. Total Environ. 511, 777–785.